

Non-destructive state detection for quantum logic spectroscopy of molecular ions

Fabian Wolf¹, Yong Wan^{1,†}, Jan C. Heip¹, Florian Gebert¹, Chunyan Shi¹ & Piet O. Schmidt^{1,2}

Precision laser spectroscopy¹ of cold and trapped molecular ions is a powerful tool in fundamental physics—used, for example, in determining fundamental constants², testing for their possible variation in the laboratory^{3,4}, and searching for a possible electric dipole moment of the electron⁵. However, the absence of cycling transitions in molecules poses a challenge for direct laser cooling of the ions⁶, and for controlling^{7–11} and detecting their quantum states. Previously used state-detection techniques based on photodissociation¹² or chemical reactions¹³ are destructive and therefore inefficient, restricting the achievable resolution in laser spectroscopy. Here, we experimentally demonstrate non-destructive detection of the quantum state of a single trapped molecular ion through its strong Coulomb coupling to a well controlled, co-trapped atomic ion. An algorithm based on a state-dependent optical dipole force¹⁴ changes the internal state of the atom according to the internal state of the molecule. We show that individual quantum states in the molecular ion can be distinguished by the strength of their coupling to the optical dipole force. We also observe quantum jumps (induced by black-body radiation) between rotational states of a single molecular ion. Using the detuning dependence of the state-detection signal, we implement a variant of quantum logic spectroscopy^{15,16} of a molecular resonance. Our state-detection technique is relevant to a wide range of molecular ions, and could be applied to state-controlled quantum chemistry¹⁷ and to spectroscopic investigations of molecules that serve as probes for interstellar clouds^{18,19}.

One of the salient features of trapped-ion systems is that the universal Coulomb interaction allows strong coupling of diverse quantum objects—such as different species of atomic ions, or of atomic and molecular ions. Being able to perform quantum logic operations (for example, in the form of gates^{14,20,21}) between such quantum objects has proven useful for quantum information processing and quantum simulations. The use of quantum logic operations in trapped-ion systems also allows the advantages of different atomic species to be combined. Quantum logic spectroscopy is one application, in which the high degree of control achieved over selected atomic ions is extended to species over which such control is lacking^{15,16}. Here, we demonstrate quantum logic operations between a single molecular ion and a co-trapped atomic ion. Our findings make a wide range of molecular ions accessible to quantum logic operations. Our technique also allows single molecules to be investigated in a well isolated system without being disturbed by the environment (the limiting factor in other implementations of single-molecule spectroscopy, such as surface-enhanced Raman spectroscopy²²).

Quantum logic operations between atoms are based on quantum-state-dependent forces, often induced by laser fields. The same approach is applicable to molecular ions. Unlike with atomic ions, however, the laser coupling to the molecular ion is distributed over many rotational–vibrational transitions, which weakens the interaction

strength for individual transitions (see Methods). The strength of the optical dipole force (ODF) on the molecular ion is inversely proportional to the detuning of the dipole laser from an optical transition in the ion. This transition frequency depends on the rotational state of the molecule. By measuring the strength of the dipole force, we can thus infer the rotational state. If the strength of this force is oscillating with a frequency close to one of the secular motional frequencies of a two-ion crystal (consisting of a molecular and an atomic ion), it is resonantly enhanced, generating coherent states of motion, which can be detected on the atomic ion^{23–25}.

Here, we extend this simple detection scheme. We detect the small ODF that arises from a laser field tuned near the $X^1\Sigma^+(J=1) \rightarrow A^1\Sigma^+(J=0)$ resonance (detuning Δ_{MgH}) in a $^{24}\text{MgH}^+$ molecular ion, in the presence of a background force (which is nearly independent of detuning) from a co-trapped $^{25}\text{Mg}^+$ atomic ion (Fig. 1c; $X^1\Sigma^+$ and $A^1\Sigma^+$ label the molecular energy levels, and the superscript ‘1’ refers to the multiplicity of the electron spin). Black-body radiation induces transitions between rotational states (J), resulting in a thermal rotational-state population with a maximum at $J=4$ for temperatures near 300 K. We chose to probe the $J=1$ state (which makes up around 8% of the population of rotational states), because of its long average dwell time of around 3 seconds (see Extended Data Fig. 1). The vibrational population with vibrational quantum number $\nu > 0$ in $^{24}\text{MgH}^+$ is negligible at room temperature, owing to the large vibrational spacing²⁶. Applying the ODF resonant with either the in-phase or the out-of-phase mode implements a displacement operator that results in coherent states of motion²⁵, which are impractical for state discrimination because of their non-orthogonality. Instead, we map the molecule’s internal state information to an engineered motional two-level quantum system (motional qubit) that is coupled by the ODF. This approach allows us to suppress the background force from $^{25}\text{Mg}^+$ and enables advanced coherent-population-transfer schemes, such as composite pulses²¹.

The state-detection algorithm starts with both axial motional modes of the two-ion crystal (which consists of a $^{25}\text{Mg}^+$ and a $^{24}\text{MgH}^+$ ion) initialized in the motional ground state $|0\rangle_{\text{m}} \equiv |0\rangle_{\text{IP}}|0\rangle_{\text{OP}}$ via the atomic ion²⁷. (‘IP’ denotes ‘in-phase’; ‘OP’ denotes ‘out-of-phase’). Two long-lived hyperfine states in $^{25}\text{Mg}^+$ serve as the atomic qubit denoted by $|\downarrow\rangle_{\text{Mg}}$, $|\uparrow\rangle_{\text{Mg}}$ (Fig. 1a), initialized to $|\downarrow\rangle_{\text{Mg}}$. The motional qubit is prepared in the state $|\downarrow\rangle_{\text{m}} \equiv |1\rangle_{\text{IP}}|0\rangle_{\text{OP}}$ by driving a π -pulse on the blue sideband transition (BSB) of the in-phase mode on the atomic ion while changing its internal state from $|\downarrow\rangle_{\text{Mg}}$ to $|\uparrow\rangle_{\text{Mg}}$. The ODF is implemented by applying two counter-propagating laser beams along the axial direction of the ion trap, forming an oscillating one-dimensional optical lattice. By adjusting the relative detuning, δ , between the two beams to the difference between the motional frequencies of the axial in-phase and out-of-phase modes, $\delta = \omega_{\text{OP}} - \omega_{\text{IP}} = \omega_{\text{IP}}(\sqrt{3} - 1)$, a Raman coupling involving only the motional states $|\downarrow\rangle_{\text{m}} \leftrightarrow |\uparrow\rangle_{\text{m}} \equiv |0\rangle_{\text{IP}}|1\rangle_{\text{OP}}$ is implemented. This then results in Rabi flopping between the two composite states (Fig. 2 and Extended Data Fig. 2).

¹Physikalisch-Technische Bundesanstalt, 38116 Braunschweig, Germany. ²Institut für Quantenoptik, Leibniz Universität Hannover, 30167 Hannover, Germany. [†]Present address: National Institute of Standards and Technology, 325 Broadway, Boulder, Colorado 80305, USA.

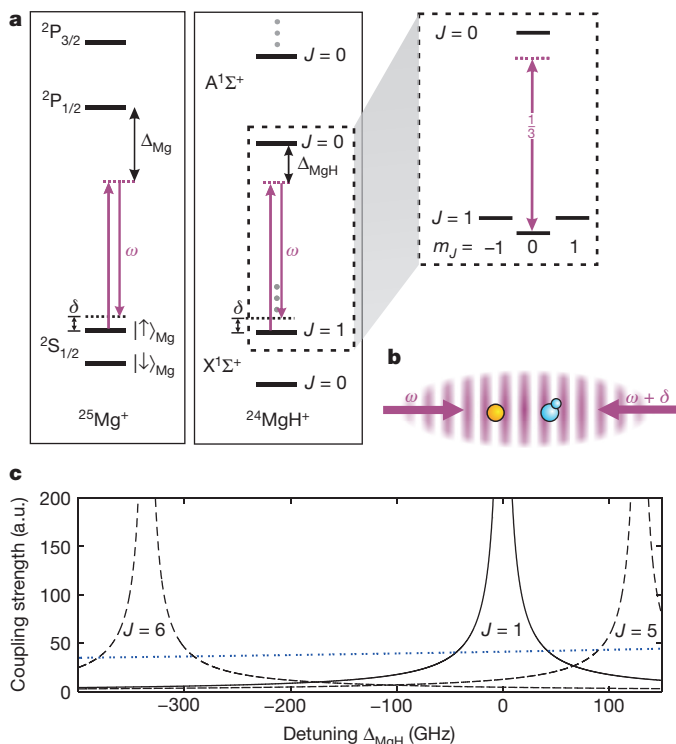


Figure 1 | Coupling strength of an optical dipole force to the atomic and molecular ions. **a**, Partial level scheme of the relevant atomic (left) and molecular states (right) and their laser coupling to the lattice laser. J refers to the rotational state; ω is the laser frequency; $^2P_{3/2}$, $^2P_{1/2}$, $^2S_{1/2}$, $A^1\Sigma^+$ and $X^1\Sigma^+$ are atomic/molecular energy levels, with the superscripts denoting the multiplicity of the electron spin; Δ_{Mg} and Δ_{MgH} represent the amount of detuning from atomic/molecular resonance; δ represents the relative detuning of the two laser beams forming the optical lattice. The inset shows the molecular substructure for the states involved in our state-detection sequence. The number on the transition in the inset is the experimentally implemented geometric coupling coefficient. **b**, The two lattice beams form a moving interference pattern, leading to a temporally and spatially varying light force on both ions (yellow, $^{25}\text{Mg}^+$; blue, $^{24}\text{MgH}^+$). **c**, Rotational state (J , $m_J = 0$) and detuning-dependent coupling strength of the optical dipole force, interacting with a $^{24}\text{MgH}^+$ molecular ion on the P-branch ($J \rightarrow J-1$, solid line) and R-branch ($J \rightarrow J+1$, dashed line) of the $X^1\Sigma^+ \rightarrow A^1\Sigma^+$ electronic transition. The blue dotted line denotes the coupling strength to the $^{25}\text{Mg}^+$ ion.

The interaction between the lattice laser field and the motional qubit is described by the Hamiltonian (see Methods):

$$H = \hbar\Omega_{\text{eff}}\eta_{\text{IP}}\eta_{\text{OP}}(a_{\text{IP}}a_{\text{OP}}^\dagger + a_{\text{IP}}^\dagger a_{\text{OP}}) \quad (1)$$

where $a_{\text{IP(OP)}}^\dagger/a_{\text{IP(OP)}}$ is the creation/annihilation operator for the in-phase (or out-of-phase) mode, $\eta_{\text{IP(OP)}}$ is the Lamb–Dicke parameter for the in-phase (or out-of-phase) mode²⁷, \hbar is Planck's constant divided by 2π ; and Ω_{eff} is the effective Rabi frequency. It is given by:

$$\Omega_{\text{eff}} = \Omega_{\text{Mg}} \sqrt{1 - 2R(\Delta_{\text{MgH}})\cos(\delta\varphi) + R(\Delta_{\text{MgH}})^2} \quad (2)$$

where $R(\Delta_{\text{MgH}}) = \Omega_{\text{MgH}}(\Delta_{\text{MgH}})/\Omega_{\text{Mg}}$ is the ratio between the Rabi frequencies of the Raman couplings in the molecular and atomic ions, depending on the detuning Δ_{MgH} . The distance between the ions determines the relative phase, $\delta\varphi$, between the forces on the ions¹⁴. In a Bloch-sphere picture, the effect of the ODF on the atom and the molecule can be illustrated as the vector sum of two torques, $\mathbf{F}_{\text{ODF}} = \mathbf{F}_{\text{Mg}} + \mathbf{F}_{\text{MgH}}$, acting on the motional qubit (Fig. 2b, c). In the experiment, the time, t_{latt} , in which the lattice laser interacts with the ions is adjusted such that for $\Omega_{\text{MgH}} = 0$ (that is, the molecular ion is not in $J = 1$) a π -pulse is performed on the motional qubit (Fig. 2b). If the

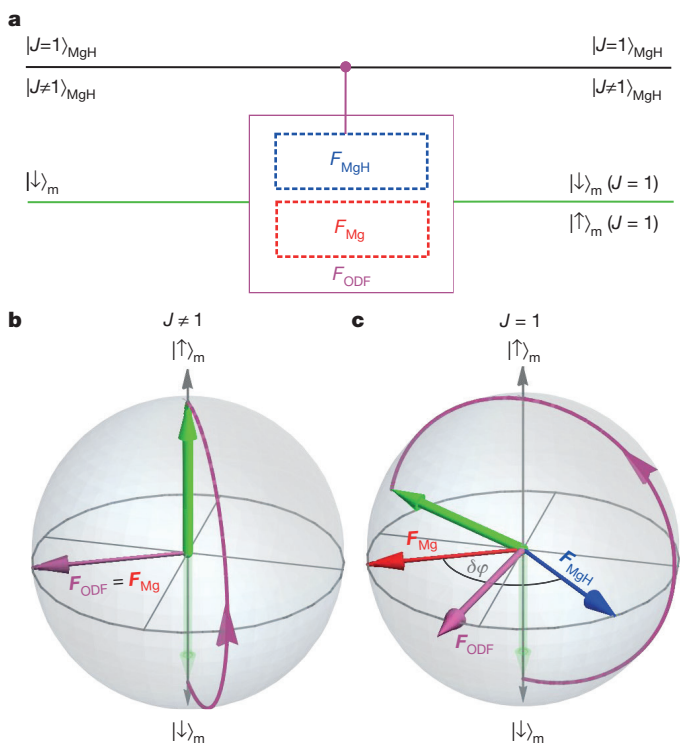


Figure 2 | Mapping of the molecular state to the motional qubit.

a, Circuit description of the mapping process. For ideally chosen parameters Δ_{MgH} and $\delta\varphi$, the circuit is equivalent to a CNOT. The action of the optical dipole force (ODF) on the motional qubit is represented by the torque $\mathbf{F}_{\text{ODF}} = \mathbf{F}_{\text{Mg}} + \mathbf{F}_{\text{MgH}}$. **b**, For $J \neq 1$, only the atomic ion interacts with the lattice. The ODF creates a torque, \mathbf{F}_{Mg} , on the Bloch sphere (purple arrows). **c**, If $J = 1$, the additional force on the molecule (torque \mathbf{F}_{MgH} , depicted in blue) is added to the force on the atom, leading to a modified population transfer.

molecule is in the probed state ($\Omega_{\text{MgH}} \neq 0$), the additional force changes the population transfer (Fig. 2c). This step transfers the internal information of the molecular state to the motional qubit. The second BSB π -pulse maps the motional-state population (containing the molecule's internal state information) to the atomic qubit. The population in state $|\downarrow\rangle_{\text{Mg}}$ follows:

$$P_{|\downarrow\rangle_{\text{Mg}}} = \frac{1}{2} \left[1 + \cos\left(\pi\sqrt{1 - 2R(\Delta_{\text{MgH}})\cos(\delta\varphi) + R(\Delta_{\text{MgH}})^2}\right) \right] \quad (3)$$

and is detected using state-dependent fluorescence on the $^{25}\text{Mg}^+$ ion, where $|\downarrow\rangle_{\text{Mg}}$ fluoresces and $|\uparrow\rangle_{\text{Mg}}$ does not. The full sequence is shown in Extended Data Fig. 3.

The calculated signal $P_{|\downarrow\rangle_{\text{Mg}}}$ is shown in Fig. 3a for different phases ($\delta\varphi$) and different detuning Δ_{MgH} values. The maxima correspond to rotations of $2\pi n$ on the Bloch sphere of the motional qubit, with $n \in \mathbb{N}$. In particular, at the outermost peaks (Fig. 3b), the forces from the atomic and molecular ions cancel or add up to 2π exactly, depending on the sign of Δ_{MgH} . There is a trade-off in the choice of lattice-laser detuning from the molecular resonance. That is, if the detuning is too large, the ODF will not be detectably different for a molecule in the rotational state of interest compared with a molecule in any other state. For a detuning too small, spontaneous Raman scattering will change the rotational state before it can be detected. Under ideal experimental conditions, it is possible to choose a combination of the phase $\delta\varphi$ and the detuning Δ_{MgH} to perform state detection in a single experimental repetition (cycle), because it is free from quantum projection noise ($P_{|\downarrow\rangle_{\text{Mg}}} = 1$ if the molecule is in $J = 1$, and $P_{|\downarrow\rangle_{\text{Mg}}} = 0$ if it is not). In this case, the experimental sequence can be understood in terms of a CNOT gate acting on the motional qubit with the molecular rotational qubit $|J\rangle_{\text{MgH}}$ as a control (Fig. 2a):

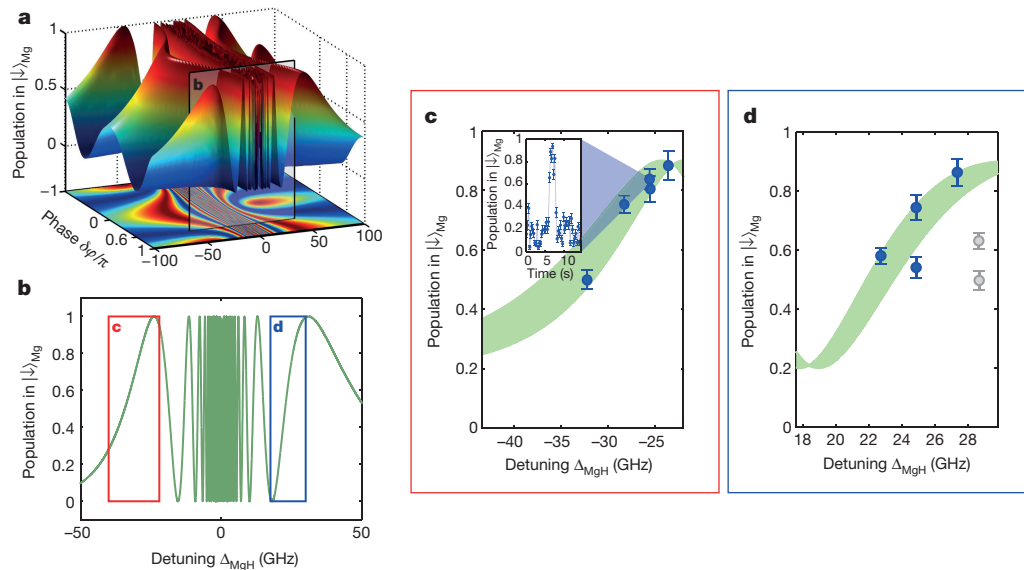


Figure 3 | Non-destructive state detection. **a**, The theoretically calculated signal $P_{|\downarrow\rangle_{\text{Mg}}}$ on the atomic ion (that is, the proportion of the population that is in the $|\downarrow\rangle_{\text{Mg}}$ state), for $^{24}\text{MgH}^+$ in the $|J=1, m_J=0\rangle_{\text{MgH}}$ state, and its dependence on the relative phase, $\delta\varphi$, of the optical force between the atomic and molecular ion, and on the detuning, Δ_{MgH} , from molecular resonance. **b**, Cross-section of panel **a**, for the phase $\delta\varphi \approx 0.6\pi$, corresponding to a trap frequency of $\omega_{\text{TP}} \approx 2.17$ MHz. **c**, **d**, The height of the observed signals as a function of detuning for the regions indicated in **b**. The inset in **c** shows a

$$|J \neq 1\rangle_{\text{MgH}} |\downarrow\rangle_{\text{m}} \rightarrow |J \neq 1\rangle_{\text{MgH}} |\uparrow\rangle_{\text{m}}$$

$$|J \neq 1\rangle_{\text{MgH}} |\uparrow\rangle_{\text{m}} \rightarrow |J \neq 1\rangle_{\text{MgH}} |\downarrow\rangle_{\text{m}}$$

$$|J=1\rangle_{\text{MgH}} |\downarrow\rangle_{\text{m}} \rightarrow |J=1\rangle_{\text{MgH}} |\downarrow\rangle_{\text{m}}$$

$$|J=1\rangle_{\text{MgH}} |\uparrow\rangle_{\text{m}} \rightarrow |J=1\rangle_{\text{MgH}} |\uparrow\rangle_{\text{m}}$$

A typical measurement with a positive detection event can be seen in the inset of Fig. 3c. If the molecular ion is not in the probed rotational state, the π -pulse on the motional qubit is successful and we observe low fluorescence, ($P_{|\downarrow\rangle_{\text{Mg}}} \approx 0$). After entering the $J=1$ state, the additional force on the molecule will change the π -time on the motional qubit and we observe fluorescence on the $^{25}\text{Mg}^+$ ion ($P_{|\downarrow\rangle_{\text{Mg}}} > 0$), until the rotational state changes again. The signal corresponds to a quantum jump of the rotational state in the molecular ion, induced by black-body radiation. The signal background of $P_{|\downarrow\rangle_{\text{Mg}}} \approx 0.2$ and reduced contrast arises from experimental imperfections in implementing the logic gates (see Methods). Because the algorithm implements a quantum non-demolition measurement of the molecular state, we reduce quantum projection noise by averaging each data point over 30 experimental cycles with a duration of about 9.3 milliseconds per cycle. We identified an experimental event as a positive detection event if at least three consecutive data points were significantly (1.5σ) above background (see Methods). In a total measuring time of approximately 23 hours, we observed 18 positive detection signals of up to several seconds' duration. The estimated average number of scattered photons from the optical lattice beams that interact with the molecular ion during a single detection cycle at $\Delta_{\text{MgH}} = 25$ GHz is around 0.04 (see Methods). If we assume that a single scattered photon removes the molecule from its rotational state, this results in an average single-cycle detection efficiency of 96%, neglecting imperfections in any of the qubit and gate operations; this therefore represents an upper bound. Estimates of the expected number of events—calculated using this detection efficiency, the mean population and the required averaging time of about 1 second

typical measurement result for a quantum jump (driven by black-body radiation) into and out of the $J=1$ rotational state. The error bars (68% confidence interval) are dominated by quantum projection noise. The thickness of the theory bands (green areas in **c**, **d**) accounts for small changes in trap frequency (and thus in $\delta\varphi$) for the different data points. The grey data points are excluded from the analysis in Fig. 4, because they could not be assigned to a specific slope of the theoretical prediction, thus preventing unambiguous inversion of equation (3).

for a positive signal event—agree well with the experimental results (see Methods).

The lattice light introduces an AC Stark shift in the molecule's spectral lines of the order of several hundred kilohertz, which is much larger than all magnetic couplings in the molecular ion. Therefore, the substates are labelled by m_J with the quantization axis along the electric-field direction of the lattice light. In this coordinate system, only π -polarized light is present, coupling only to states with $m_J=0$ (Fig. 1a inset). The resulting signal as a function of the detuning and the molecular quantum state is shown in Fig. 3c, d for $\delta\varphi \approx 0.6\pi$, corresponding to a normal mode frequency of $\omega_{\text{TP}} \approx 2.17$ MHz. Experimental data for $\delta\varphi \approx 0$ are shown in Extended Data Fig. 4.

The dependence of $R(\Delta_{\text{MgH}})$ on the detuning Δ_{MgH} from a molecular resonance allows us to perform spectroscopy, because forces arising from coupling to other rotational states are negligible over a large range of detunings (Fig. 1b). For this, we have combined data taken for different detuning Δ_{MgH} values and different phases ($\delta\varphi$) by inverting equation (3) numerically and accounting for the reduced contrast (Extended Data Fig. 2). The measured Rabi frequency ratios, $R(\Delta_{\text{MgH}})$, for the $X^1\Sigma^+(J=1) \rightarrow A^1\Sigma^+(J=0)$ transition are summarized in Fig. 4. Also shown in Fig. 4 is a fit to the wings of a simplified model, $R_{\text{fit}}(f) = A/|f-f_0|$, with the free parameters A and f_0 , where we assumed a detuning-independent background coupling to the far-detuned transition in the $^{25}\text{Mg}^+$ ion (Fig. 1c). We determine the transition frequency to be $f_0 = 1067.74789(40)$ THz (68% confidence interval), which is in agreement with a previous measurement of $f_0 = 1067.7473(15)$ THz (ref. 26). The fitted characteristic detuning for the Rabi frequency ratio is $A = 45.98(73)$ GHz (68% confidence interval).

We estimate that non-destructive detection of the internal state of a molecular ion with near 100% efficiency could take less than 10 milliseconds, given a larger detuning Δ_{MgH} of roughly 100 GHz and improvements in preparing and manipulating the co-trapped atomic ion (see Methods). This represents a major advance over previous, destructive detection techniques, which require frequent reloading. Our technique will realise its potential in high-precision spectroscopic investigations of narrow transitions between states in molecules using an independent spectroscopy laser. However, whereas in our present

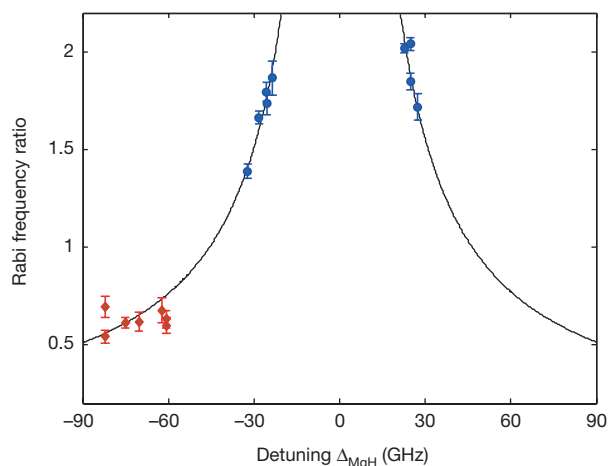


Figure 4 | Quantum logic spectroscopy. The Rabi frequency ratio, $R = \Omega_{\text{MgH}}(\Delta_{\text{MgH}})/\Omega_{\text{Mg}}$, as a function of detuning Δ_{MgH} from a molecular resonance, for all data for which equation (3) could be inverted unambiguously (see Fig. 3c, d). Measurement data recorded at $\omega_{\text{IP}} \approx 2.17$ MHz ($\delta\varphi \approx 0.6\pi$; nine points; see Fig. 3) and $\omega_{\text{IP}} \approx 2.21$ MHz ($\delta\varphi \approx 0$; seven points; see Extended Data Fig. 4) are indicated by blue circles and red diamonds, respectively. The solid line is a fit to the combined data set, resulting in $f_0 = 1067.74789(40)$ THz. The error bars correspond to the errors shown in Fig. 3 and Extended Data Fig. 4 (68% confidence intervals).

work black-body radiation probabilistically populates the detected state, precision spectroscopy will require more-efficient state-preparation schemes^{28,29} or rotational-vibrational cooling techniques^{7–11}. A combination of these tools will enable the realization of optical clocks based on molecular ions approaching fractional frequency uncertainties at the 10^{-18} level³⁰—where the underlying clock transitions, or combinations of transitions, can be sensitive to variations in fundamental constants³, to an electron electric dipole moment⁵, or to parity violation in chiral molecules.

Online Content Methods, along with any additional Extended Data display items and Source Data, are available in the online version of the paper; references unique to these sections appear only in the online paper.

Received 30 June; accepted 27 November 2015.

Published online 8 February 2016.

1. Germann, M., Tong, X. & Willitsch, S. Observation of electric-dipole-forbidden infrared transitions in cold molecular ions. *Nature Phys.* **10**, 820–824 (2014).
2. Koelemeij, J., Roth, B., Wicht, A., Ernsting, I. & Schiller, S. Vibrational spectroscopy of HD^+ with 2-ppb accuracy. *Phys. Rev. Lett.* **98**, 173002 (2007).
3. Schiller, S. & Korobov, V. Tests of time independence of the electron and nuclear masses with ultracold molecules. *Phys. Rev. A* **71**, 032505 (2005).
4. Flambaum, V. & Kozlov, M. Enhanced sensitivity to the time variation of the fine-structure constant and m_p/m_e in diatomic molecules. *Phys. Rev. Lett.* **99**, 150801 (2007).
5. Loh, H. *et al.* Precision spectroscopy of polarized molecules in an ion trap. *Science* **342**, 1220–1222 (2013).
6. Shuman, E. S., Barry, J. F. & DeMille, D. Laser cooling of a diatomic molecule. *Nature* **467**, 820–823 (2010).
7. Rellergert, W. G. *et al.* Evidence for sympathetic vibrational cooling of translationally cold molecules. *Nature* **495**, 490–494 (2013).
8. Schneider, T., Roth, B., Duncker, H., Ernsting, I. & Schiller, S. All-optical preparation of molecular ions in the rovibrational ground state. *Nature Phys.* **6**, 275–278 (2010).

9. Staunum, P. F., Højbjerg, K., Skyt, P. S., Hansen, A. K. & Drewsen, M. Rotational laser cooling of vibrationally and translationally cold molecular ions. *Nature Phys.* **6**, 271–274 (2010).
10. Lien, C.-Y. *et al.* Broadband optical cooling of molecular rotors from room temperature to the ground state. *Nature Commun.* **5**, 4783 (2014).
11. Hansen, A. K. *et al.* Efficient rotational cooling of Coulomb-crystallized molecular ions by a helium buffer gas. *Nature* **508**, 76–79 (2014).
12. Højbjerg, K., Hansen, A. K., Skyt, P. S., Staunum, P. F. & Drewsen, M. Rotational state resolved photodissociation spectroscopy of translationally and vibrationally cold MgH^+ ions: toward rotational cooling of molecular ions. *New J. Phys.* **11**, 055026 (2009).
13. Tong, X., Winney, A. & Willitsch, S. Sympathetic cooling of molecular ions in selected rotational and vibrational states produced by threshold photoionization. *Phys. Rev. Lett.* **105**, 143001 (2010).
14. Leibfried, D. *et al.* Experimental demonstration of a robust, high-fidelity geometric two ion-qubit phase gate. *Nature* **422**, 412–415 (2003).
15. Schmidt, P. O. *et al.* Spectroscopy using quantum logic. *Science* **309**, 749–752 (2005).
16. Wan, Y. *et al.* Precision spectroscopy by photon-recoil signal amplification. *Nature Commun.* **5**, 4096 (2014).
17. Ratschbacher, L., Zipkes, C., Sias, C. & Köhl, M. Controlling chemical reactions of a single particle. *Nature Phys.* **8**, 649–652 (2012).
18. Brünken, S. *et al.* H_2D^+ observations give an age of at least one million years for a cloud core forming Sun-like stars. *Nature* **516**, 219–221 (2014).
19. Campbell, E. K., Holz, M., Gerlich, D. & Maier, J. P. Laboratory confirmation of C_{60}^+ as the carrier of two diffuse interstellar bands. *Nature* **523**, 322–323 (2015).
20. Cirac, J. I. & Zoller, P. Quantum computations with cold trapped ions. *Phys. Rev. Lett.* **74**, 4091 (1995).
21. Schmidt-Kaler, F. *et al.* Realization of the Cirac-Zoller controlled-NOT quantum gate. *Nature* **422**, 408–411 (2003).
22. Nie, S. & Emory, S. R. Probing single molecules and single nanoparticles by surface-enhanced Raman scattering. *Science* **275**, 1102–1106 (1997).
23. Schmidt, P. O. *et al.* in *Proceedings of Non-Neutral Plasma Physics VI, Workshop on Non-Neutral Plasmas*, Vol. 862 (eds Drewsen, M., Uggerhøj, U. & Knudsen, H.) 305–312 (Aarhus, 2006).
24. Vogelius, I. S., Madsen, L. B. & Drewsen, M. Probabilistic state preparation of a single molecular ion by projection measurement. *J. Phys. At. Mol. Opt. Phys.* **39**, S1259–S1265 (2006).
25. Hume, D. B. *et al.* Trapped-ion state detection through coherent motion. *Phys. Rev. Lett.* **107**, 243902 (2011).
26. Balfour, W. J. Rotational analysis of the $A^1\Sigma^+ \rightarrow X^1\Sigma^+$ and $B^1\Pi \rightarrow X^1\Sigma^+$ systems of $^{24}\text{MgH}^+$, $^{25}\text{MgH}^+$, and $^{26}\text{MgH}^+$. *Can. J. Phys.* **50**, 1082–1091 (1972).
27. Wan, Y., Gebert, F., Wolf, F. & Schmidt, P. O. Efficient sympathetic motional-ground-state cooling of a molecular ion. *Phys. Rev. A* **91**, 043425 (2015).
28. Leibfried, D. Quantum state preparation and control of single molecular ions. *New J. Phys.* **14**, 023029 (2012).
29. Ding, S. & Matsukevich, D. N. Quantum logic for the control and manipulation of molecular ions using a frequency comb. *New J. Phys.* **14**, 023028 (2012).
30. Schiller, S., Bakalov, D. & Korobov, V. I. Simplest molecules as candidates for precise optical clocks. *Phys. Rev. Lett.* **113**, 023004 (2014).

Acknowledgements We acknowledge the support of the Deutsche Forschungsgemeinschaft through QUEST and grant SCHM2678/3-1. This work was financially supported by the State of Lower-Saxony, Hannover, Germany. Y.W. acknowledges support from the Braunschweig International Graduate School of Metrology. We thank E. Tiemann, H. Knöckel, O. Dulieu and I.D. Leroux for discussions; M. Drewsen and O. Dulieu for the transition-matrix elements for $^{24}\text{MgH}^+$; and E. Tiemann, B. Hemmerling, and I.D. Leroux for reading the manuscript.

Author Contributions P.O.S. conceived and supervised the experiment. F.W. developed the read-out algorithm. F.W., J.C.H. and C.S. carried out the measurements. Y.W. performed the simulations and calculated the lattice coupling strength. F.W. and P.O.S. wrote the main part of the manuscript. Y.W. and F.G. built essential parts of the experiment. All authors discussed the results and contributed to the manuscript.

Author Information Reprints and permissions information is available at www.nature.com/reprints. The authors declare no competing financial interests. Readers are welcome to comment on the online version of the paper. Correspondence and requests for materials should be addressed to P.O.S. (piet.schmidt@quantummetrology.de).

METHODS

Experimental set-up. The experiments are carried out in a linear Paul trap, with a typical axial trap frequency of 2.21 MHz for $^{25}\text{Mg}^+$. We use a hyperfine qubit consisting of the states $|\downarrow\rangle_{\text{Mg}} = |F=3, m_F=3\rangle$ and $|\uparrow\rangle_{\text{Mg}} = |F=2, m_F=2\rangle$ of the $^2\text{S}_{1/2}$ electronic ground state (m_F is the projection of the total spin, F , on the quantization axis). The Raman laser system for coherent manipulation of the $^{25}\text{Mg}^+$ qubit via the $^2\text{P}_{3/2}$ level is based on a frequency-quadrupled fibre laser³¹. The detuning from the atomic resonance is fixed at 9.2 GHz, limiting ground-state cooling efficiency²⁷ and qubit operations owing to spontaneous Raman scattering³². The same laser is also used for internal state discrimination by applying an optical sideband tuned near resonance of the $|\downarrow\rangle_{\text{Mg}} \rightarrow |^2\text{P}_{3/2}, F=4, m_F=4\rangle$ component of the D2 transition. A similar laser system addressing the $^2\text{S}_{1/2} \rightarrow ^2\text{P}_{1/2}$ (D1) transition is used for optical repumping and quenching during sideband cooling²⁷.

The light fields creating the optical lattice for molecular-state detection and spectroscopy are provided by a frequency-doubled dye laser whose frequency is tuned close to the $X^1\Sigma^+(J=1) \rightarrow A^1\Sigma^+(J=0)$ transition of $^{24}\text{MgH}^+$, with a variable detuning Δ_{MgH} typically smaller than ~ 100 GHz from the molecular transition, and detuned by $\Delta_{\text{MgH}} \approx 1.5$ THz from the atomic D1 transition of $^{25}\text{Mg}^+$. Two counter-propagating laser beams derived from this laser are linearly polarized in the horizontal plane with a relative detuning δ . They are aligned along the trap axis to form an angle of $\pi/4$, with the atomic quantization axis being given by a static applied magnetic field of ~ 0.58 mT. The detuning between the two laser fields results in a moving optical lattice, providing a temporally and spatially varying force on the two ions with a relative phase $\delta\varphi$, which depends on the distance between the two ions. Two optical fibres suitable for ultraviolet single-mode transmission³³ are used to reduce the effect of beam-pointing fluctuations on the coupling strength, and aid in the initial alignment of the beams onto the molecular ion. The frequency of the spectroscopy light is monitored by a commercial wavemeter (High Finesse WS/7). We assign an uncertainty of less than 100 MHz to the measured value.

To reduce quantum projection noise resulting from imperfect single-qubit operations, we average over 30 measurement cycles to get a single measurement point. This procedure takes 280 ms. If at least three consecutive points are significantly above the threshold (1.5σ), we assign them to a positive detection signal from the molecule. To determine the signal height, we take the first and last measurement points into account only if they are at least 2σ above the background. This procedure improves the signal quality, because we remove data points that contain only a fraction of positive detection events during the 30 repetitions.

Hamiltonian for lattice coupling. The Hamiltonian (H) for N ions coupled by a one-dimensional moving optical lattice in the interaction picture can be written as:

$$H = \sum_j^N \hbar\Omega_j e^{-i(\delta t - \varphi_j)} \exp\left[\sum_k^N i\eta_{jk}(a_k e^{-i\omega_k t} + a_k^\dagger e^{i\omega_k t})\right] + \text{h.c.}$$

where j labels the ions; k labels the axial motional modes with frequency ω_k ; η_{jk} is the Lamb–Dicke parameter; a_k^\dagger is the creation operator; h.c. is the hermitean conjugate; φ_j is a phase. $\Omega_j = \Omega_{1j}\Omega_{2j}/(2\Delta)$ is the two-photon Rabi frequency for the two lattice beams coupling to an electronically excited state with detuning Δ . Considering the case of two ions $j \in \{1, 2\}$, we have to take two axial motional modes into account, namely $k \in \{\text{IP}, \text{OP}\}$, denoting the in-phase and out-of-phase motion of the two ions, respectively. In the following, the relative detuning of the two lattice beams, δ , is chosen to be $\delta = \omega_{\text{OP}} - \omega_{\text{IP}}$. After the rotating wave approximation, only the second-order mixed term in the Lamb–Dicke approximation survives, resulting in the following interaction Hamiltonian, mediating the coupling between the two modes:

$$H = - \sum_{j=1,2} \hbar\Omega_j e^{i\varphi_j} \eta_{j,\text{IP}} \eta_{j,\text{OP}} a_{\text{IP}}^\dagger a_{\text{OP}} + \text{h.c.}$$

In adding up the forces on the two ions, we have to consider the different effect on both modes, and take into account the signs in the matrix for transformation between normal modes and laboratory frame³⁴. We find for two ions with equal mass the Lamb–Dicke factors:

$$\eta_{1,\text{IP}} = \eta_{2,\text{IP}} \equiv \eta_{\text{IP}}$$

$$\eta_{1,\text{OP}} = -\eta_{2,\text{OP}} \equiv \eta_{\text{OP}}$$

and the Hamiltonian reads:

$$H = -\hbar\eta_{\text{IP}}\eta_{\text{OP}} a_{\text{IP}}^\dagger a_{\text{OP}} [\Omega_1 e^{i\varphi_1} - \Omega_2 e^{i\varphi_2}] + \text{h.c.}$$

It is convenient to define:

$$\delta\varphi \equiv \varphi_1 - \varphi_2$$

$$\Phi \equiv \varphi_1 + \varphi_2$$

The Hamiltonian can then be written as:

$$H = -e^{i\Phi/2} \hbar\eta_{\text{IP}}\eta_{\text{OP}} a_{\text{IP}}^\dagger a_{\text{OP}} [\Omega_1 e^{i\delta\varphi/2} - \Omega_2 e^{-i\delta\varphi/2}] + \text{h.c.}$$

We introduce the modified Rabi frequency:

$$\Omega = \Omega_{\text{eff}} e^{i\Phi/2} \equiv -e^{i\Phi/2} [\Omega_1 e^{i\delta\varphi/2} - \Omega_2 e^{-i\delta\varphi/2}]$$

with amplitude:

$$\Omega_{\text{eff}} = \Omega_2 \sqrt{1 - 2R\cos(\delta\varphi) + R^2}$$

where $R = \Omega_1/\Omega_2$ is the ratio between the Rabi frequencies and Φ_{eff} is an effective phase. Identifying $\Omega_1 = \Omega_{\text{MgH}}$ and $\Omega_2 = \Omega_{\text{Mg}}$ with the Raman Rabi frequencies for the molecular and atomic ions, respectively, we arrive at equation (2) of the main text. For very large detunings from either the atomic or the molecular ion, the effective Rabi frequency reduces to Ω_{MgH} and Ω_{Mg} , respectively. The final interaction Hamiltonian is then given by:

$$H = \hbar\Omega_{\text{eff}} \eta_{\text{IP}} \eta_{\text{OP}} (e^{i\Phi_{\text{eff}}} a_{\text{IP}}^\dagger a_{\text{OP}} + e^{-i\Phi_{\text{eff}}} a_{\text{IP}}^\dagger a_{\text{OP}}) \quad (4)$$

which is a Hamiltonian that describes a system consisting of $n+1$ coupled levels, where n is the number of initial excitations. In the case $n=1$, we get a two-level system consisting of the states $|\downarrow\rangle_{\text{M}} \equiv |1\rangle_{\text{IP}}|0\rangle_{\text{OP}}$, $|\uparrow\rangle_{\text{M}} \equiv |0\rangle_{\text{IP}}|1\rangle_{\text{OP}}$, which are coupled with the Rabi frequency Φ_{eff} . The action of this Hamiltonian can be described as Rabi flopping between motional states. Results from an experimental implementation are shown in Extended Data Fig. 2 for a two-ion crystal consisting of a $^{25}\text{Mg}^+$ ion and a molecular ion in a rotational state not addressed by the lattice. The reduced initial contrast and its decay are attributed to imperfect ground-state cooling, off-resonant scattering of the Raman beams that are interacting with the atom, and dephasing of the lattice beams. Starting from both axial modes near the ground state, a quantum of motion is added using a BSB π -pulse. The lattice coupling is then switched on for a variable time and the motional information is mapped back onto the electronic qubit by a second BSB π -pulse (see Extended Data Fig. 3). In such a sequence, we are not sensitive to the phase factors, $e^{\pm i\Phi_{\text{eff}}}$, which can therefore be neglected in the Hamiltonian, resulting in equation (1) of the main text. Note that an additional phase of π is introduced if the sign of the detuning differs for the atomic and molecular resonances, so the relative phase is given by:

$$\delta\varphi = \begin{cases} 2\pi d\Delta k \\ 2\pi\left(d\Delta k + \frac{1}{2}\right) \end{cases}$$

where d is the distance between ions and $\Delta k = k_1 - k_2 \approx 2k_1$ is the difference between the wavenumbers of the two lattice beams (the top part of the equation relates to the same sign, and the bottom part to the opposite sign).

Coupling of the optical lattice to the molecular ion. The coupling strength of the lattice laser to the molecular ion can be described by the transition matrix element between two states, $|\xi''\Lambda''\nu''J''m''_j\rangle$ and $|\xi'\Lambda'\nu'J'm'_j\rangle$, with Λ being the projection of the angular momentum on the molecular axis, which is $\Lambda' = \Lambda'' = 0$ for both involved states, since we have a $\Sigma \rightarrow \Sigma$ transition without electron angular momentum. The electronic part of the wavefunctions is given by $\xi' = A$ and $\xi'' = X$ in spectroscopic notation. The vibrational and rotational quantum numbers are given by ν and J , respectively, and m_j is the projection of J onto the quantization axis. Note that the quantization axis for the molecule is given by the electric field of the lattice light, since the AC Stark shift causes dominant-level splitting. The transition-dipole matrix element is usually approximated by:

$$\langle \xi'\nu'J'm'_j | \Lambda' | d_q | \xi''\nu''J''m''_j \rangle =$$

$$\mu_{\text{XA}} \sqrt{S^{\text{FC}}(\nu', \nu'') S^{\text{HL}}(J', \Lambda'; J'', \Lambda'') S^{\text{geom}}(J', m'_j; J'', m''_j)}$$

where μ_{XA} is the electronic transition dipole moment. The Franck–Condon factor describing the overlap of the wave functions of the two vibrational ground states can be calculated from the data given in ref. 36:

$$S^{\text{FC}}(\nu' = 0, \nu'' = 0) = \left| \int \psi_{\nu'=0}^* \psi_{\nu''=0} d\mathbf{r} \right|^2 \approx 0.0919$$

The Hönl–London factor describing the dependence of the transition strength on the rotational quantum numbers is given in ref. 37:

$$S^{\text{HL}}(J', \Lambda' = 0; J'', \Lambda'' = 0) = \max(J', J'')$$

The geometric factor describing the addition of total angular momentum of the molecule and the angular momentum of the photon is given by:

$$S_{m'_j q}^{\text{geom}}(J' m'_j; J'' m''_j) = \left| \varepsilon^q \begin{pmatrix} J' & 1 & J'' \\ -m'_j & q & m''_j \end{pmatrix}_{3j} \right|^2$$

with the Wigner 3j-symbol and the polarization components ε^q . Because the quantization axis is given by the lattice, it is convenient to calculate the coupling in a basis parallel to the lattice electric field, where the polarization components are $\varepsilon^{-1} = \varepsilon^1 = 0$ and $\varepsilon^0 = 1$.

The Rabi frequency from the interaction of the optical lattice with the molecular ion (equation (4)) starting from a specific rotational state $|\xi'' \nu'' J'' m''_j\rangle$ is given by³⁸:

$$\begin{aligned} \Omega_{\text{MgH}} &= \frac{E_1 E_2}{2\hbar^2} \sum_{m'_j} \sum_q \frac{|\varepsilon^q \langle \xi' \nu' J' m'_j | d_q | \xi'' \nu'' J'' m''_j \rangle|^2}{\Delta_{\text{MgH}}} \\ &= \frac{E_1 E_2}{2\hbar^2} \frac{\mu_{\text{XA}}^2}{\Delta_{\text{MgH}}} S^{\text{FC}} S^{\text{HL}} \sum_{m'_j} \sum_q S_{m'_j q}^{\text{geom}} \\ &= \frac{E_1 E_2}{2\hbar^2} \frac{\mu_{\text{XA}}^2}{\Delta_{\text{MgH}}} S^{\text{FC}} S^{\text{HL}} S^{\text{geom}} \end{aligned}$$

where E_1 and E_2 are the electric-field amplitudes of the two counter-propagating laser beams forming the optical lattice, and Δ_{MgH} is the detuning from the molecular resonance. Using a similar approach for the atomic ion, we get a Rabi frequency ratio that is independent of the applied electric field. From the well-known transition strengths in $^{25}\text{Mg}^+$ and the fitted value for A of 45.98(73) GHz (68% confidence interval), we extract a dipole matrix element for the molecular transition of $\mu_{\text{XA}}^{\text{exp}} = 1.2510(99)ea_0$, which is smaller than the matrix element $\mu_{\text{XA}}^{\text{th}} = 1.779ea_0$ extracted from the theoretical data presented in ref. 36. We use the experimental dipole matrix element for the curves in Fig. 3 and Extended Data Fig. 4.

Scattering rate and single-cycle detection efficiency. We assume that scattering of a single photon on the optical transition of the molecular ion will change its rotational–vibrational state, owing to the non-vanishing Franck–Condon factors between different vibrational states. Therefore, a small scattering rate is desired. In the following we use a simplified model in which the molecular ion is treated as a two-level system to estimate the order of magnitude for the spontaneous emission rate of the molecular ion that is subject to the ODF. The number of scattered photons from a two-level system, with excited-state linewidth Γ_0 , interacting for a time t_π with an optical lattice formed by two laser beams of equal Rabi frequency Ω and detuned by Δ_{Mg} from resonance is given by:

$$\Gamma_{\text{sc}} t_\pi = \frac{\Gamma_0 \Omega^2}{2\Delta_{\text{Mg}}^2} t_\pi$$

For the implemented quantum algorithm, the time t_π is chosen such that the coupling to the atomic ion drives a π -pulse between the two motional states, $t_\pi = \pi / (\Omega_{\text{Mg}} \eta_{\text{IP}} \eta_{\text{OP}})$. Using $R = \Omega_{\text{MgH}} / \Omega_{\text{Mg}}$ and $\Omega_{\text{MgH}} = \Omega^2 / (2\Delta_{\text{MgH}})$, we obtain:

$$\Gamma_{\text{sc}} t_\pi = \frac{\Gamma_0 \pi R}{\Delta_{\text{MgH}} \eta_{\text{IP}} \eta_{\text{OP}}}$$

where Γ_0 for the molecular ion is given by:

$$\Gamma_0 = \frac{\omega_0^3}{3\pi\epsilon_0\hbar, c^3} \mu_{\text{XA}}^2$$

with the scaled transition dipole moment μ_{XA} given above. For Poissonian photon distribution, the probability to scatter no photon follows:

$$P_{\text{scatt}}(0) = e^{-\Gamma_{\text{sc}} t_\pi}$$

For a detuning of roughly 25 GHz, we expect to scatter on average 0.04 photons, which corresponds to a fundamentally limited single-cycle detection efficiency of $E_{\text{ss}} = P_{\text{scatt}}(0) \approx 96\%$. For an increased detuning of -100 GHz, the number of scattered photons on average would be reduced to 0.0026 for a π -pulse with the optical lattice. However, to get a large enough signal contrast for single-cycle detection, it would be necessary to perform a 2π -pulse with the lattice, which leads to a single-cycle detection efficiency of 99.5%.

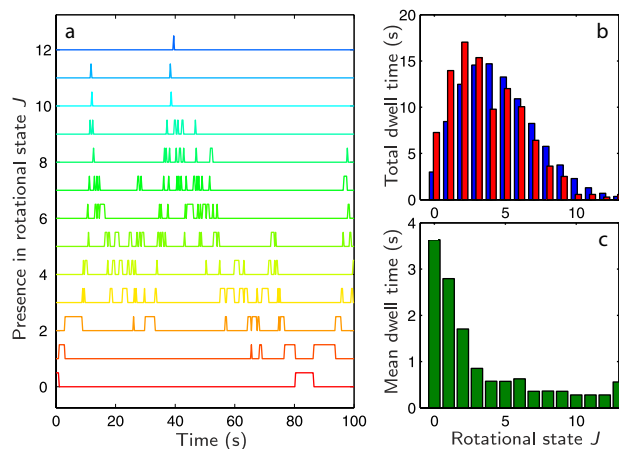
The number of positive detection events, N_{ev} , for a total number N_{total} of trials can be estimated from:

$$N_{\text{ev}} = (E_{\text{ss}})^{3N_{\text{cycle}}} P_{\text{therm}} P_{t \geq 3} N_{\text{total}}$$

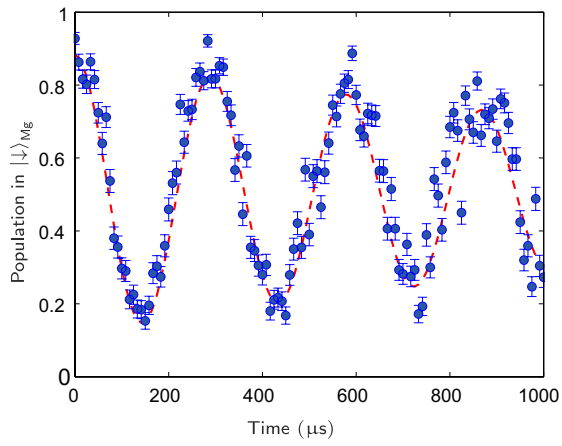
where P_{therm} is the probability of the molecule being in the probed state for a thermal distribution at 300 K, and $P_{t \geq 3}$ is the probability of the molecular ion staying at least for the time of three measurement points in the probed state, which is a prerequisite for positive detection in the experiment. In our case, we have $N_{\text{total}} \approx 2 \times 10^5$, $P_{\text{therm}} = 0.08$, $P_{t \geq 3} = 0.8$ (see Monte Carlo simulation in Extended Data Fig. 1) and $N_{\text{cycle}} = 30$. For a single-shot-detection efficiency of the order of $E_{\text{ss}} \approx 95\%$, this results in an expected number of points belonging to a detection signal of N_{ev} of about 130, which is in agreement with the observed number of points $N_{\text{ev}}^{\text{exp}} \approx 100$ assigned to the 18 positive detection events.

Uncertainties of the fitted parameters. We extracted the centre frequency and the line strength from a weighted nonlinear least-squares fit. The assigned uncertainties correspond to the 68% confidence bounds, C , that have been calculated assuming a normal distribution of errors and according to $C = b \pm t \sqrt{S}$, where b is the fitted coefficient, t is the inverse of the Student's cumulative distribution function for the required confidence, and $S = (X^T X)^{-1} s^2$, with the mean squared error s^2 and the Jacobian X of the fitted values with respect to the coefficients.

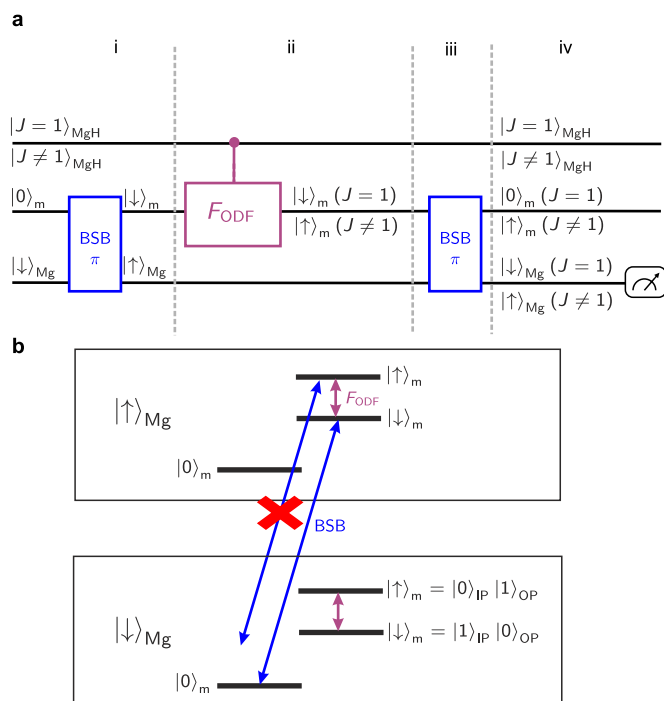
- Hemmerling, B. *et al.* A single laser system for ground state cooling of $^{25}\text{Mg}^+$. *Appl. Phys. B* **104**, 583590 (2011)
- Ozeri, R. *et al.* Hyperfine coherence in the presence of spontaneous photon scattering. *Phys. Rev. Lett.* **95**, 030403 (2005).
- Gebert, F. *et al.* Damage-free single-mode transmission of deep-UV light in hollow-core PCF. *Opt. Express* **22**, 15388–15396 (2014).
- James, D. F. V. Quantum dynamics of cold trapped ions with application to quantum computation. *Appl. Phys. B* **66**, 181–190 (1998).
- Hemmerling, B., Gebert, F., Wan, Y. & Schmidt, P. O. A novel, robust quantum detection scheme. *New J. Phys.* **14**, 023043 (2012).
- Aymar, M., Guérout, R., Sahlou, M. & Dulieu, O. Electronic structure of the magnesium hydride molecular ion. *J. Phys. At. Mol. Opt. Phys.* **42**, 154025 (2009).
- Hansson, A. & Watson, J. K. A comment on Hönl–London factors. *J. Mol. Spectrosc.* **233**, 169–173 (2005).
- Bergmann, K. & Shore, B. W. *Coherent Population Transfer*, Ch. 9 (eds Dai, H.-L. & Field, R. W.) 367 (World Scientific, 1995).



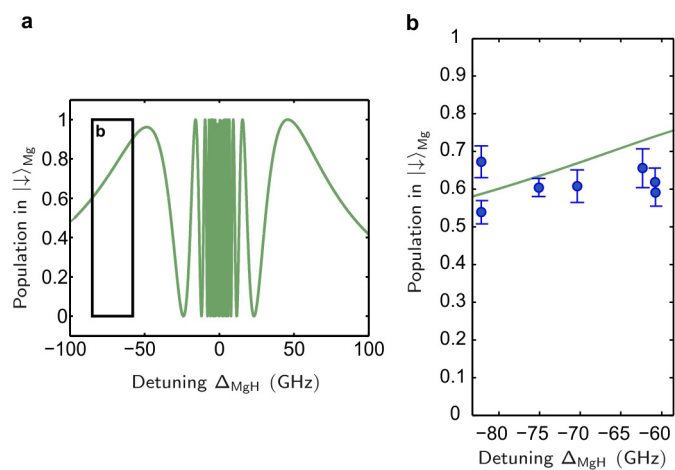
Extended Data Figure 1 | Single trajectory from a Monte Carlo simulation of molecular dynamics. **a**, The ion initially prepared in the rotational ground state is transferred to higher rotational states because of coupling to black-body radiation at 300 K. **b**, The probability of finding the ion in a certain rotational state in the simulation (red bars) follows a thermal distribution. The blue bars are calculated values from a master equation approach. The deviation between the red and blue bars results from the finite time interval of the Monte Carlo wavefunction simulation. **c**, The dwell time decreases for higher rotational states.

**Extended Data Figure 2 | Rabi flopping between motional states.**

Implementation of the sequence shown in Fig. 2 for $\Omega_{\text{MgH}} = 0$. The duration of the applied optical lattice is varied to induce Rabi flopping between the motional qubit states $|\downarrow\rangle_m$ and $|\uparrow\rangle_m$. The error bars show the 95% confidence interval of the photon-distribution fit³⁵. The red dashed line shows a fit to a damped oscillation.



Extended Data Figure 3 | Full experimental sequence. a, Circuit description of the sequence. i, A BSB π -pulse initializes the atom in the state $|\uparrow\rangle_{Mg}$ and the motional state in the qubit state $|\downarrow\rangle_m$. ii, The ODF rotates the motional qubit controlled by the internal state of the molecule (see Fig. 2). iii, A second BSB π -pulse maps the motional state (which contains the information about the molecule's internal state) to the atomic qubit. iv, The atomic qubit's state is read out by state-dependent fluorescence. **b,** Pictorial representation of the laser couplings in a simplified level scheme.



Extended Data Figure 4 | Raw data for $\delta\varphi \approx 0$. **a**, Theoretically predicted signal for $\delta\varphi \approx 0$, corresponding to $\omega_{IP} \approx 2.21$ MHz. **b**, Expansion of the region shown in **a** with the seven measured data points that are shown as red diamonds in Fig. 4. The error bars indicate the 68% confidence interval of the photon-distribution fit³⁵.